Analysis of Turbulent Scalar Flux Models for a Discrete Hole Film Cooling Flow

Julia Ling [1]
Stanford University
Mechanical Engineering Department
Stanford, CA
Email: julial@stanford.edu

Kevin J. Ryan
Stanford University
Mechanical Engineering Department
Stanford, CA

Julien Bodart
University of Toulouse
ISAE
Toulouse, France

John K. Eaton
Stanford University
Mechanical Engineering Department
Stanford, CA

ABSTRACT

Algebraic closures for the turbulent scalar fluxes were evaluated for a discrete hole film cooling geometry using the results from a high-fidelity Large Eddy Simulation (LES). Several models for the turbulent scalar fluxes exist, including the widely used Gradient Diffusion Hypothesis, the Generalized Gradient Diffusion Hypothesis, and the Higher Order Generalized Gradient Diffusion Hypothesis. By analyzing the results from the LES, it was possible to isolate the error due to these turbulent mixing models. Distributions of the turbulent diffusivity, turbulent viscosity, and turbulent Prandtl number were extracted from the LES results. It was shown that the turbulent Prandtl number varies significantly spatially, undermining the applicability of the Reynolds analogy for this flow. The LES velocity field and Reynolds stresses were fed into a RANS solver to calculate the fluid temperature distribution. This analysis revealed in which regions of the flow various modeling assumptions were invalid and what effect those assumptions had on the predicted temperature distribution.

[1] J. Ling is currently at Sandia National Labs.

Nomenclature

α_t Turbulent diffusivity

η Adiabatic effectiveness

ϕ Angle between predicted turbulent scalar fluxes and LES turbulent scalar fluxes

ν Molecular viscosity

ν_t Eddy viscosity

τ Turbulent time scale

θ Non-dimensional temperature, $\frac{T-T_{main}}{T_{cool}-T_{main}}$

C_{GGDH} Model coefficient for GGDH model

C_{HOGGDH} Model coefficient for HOGGDH model

$GGDH$ Generalized Gradient Diffusion Hypothesis

$HOGGDH$ Higher Order Generalized Gradient Diffusion Hypothesis

Pr_t Turbulent Prandtl number

T_{aw} Adiabatic wall temperature

T_{cool} Temperature at the coolant inlet

T_{main} Temperature at the main flow inlet

u_i i^{th} component of velocity

U_b Bulk-averaged main flow velocity

Introduction

In order to determine the performance of a film cooling configuration, Reynolds Averaged Navier Stokes (RANS) solvers must calculate the fluid temperature distribution. These solvers require a closure for the turbulent scalar flux term, $\overline{u_i'\theta'}$, which represents the transport of heat by turbulent fluctuations. A variety of closure schemes exist, the most widely used of which is the Gradient Diffusion Hypothesis (GDH). This model represents the turbulent scalar fluxes as shown in Eqn. 1.

$$\overline{u_i'\theta'}_{GDH} = -\alpha_t \frac{d\bar{\theta}}{dx_i} \tag{1}$$

u_i is the i^{th} component of velocity and overbars indicate a time average. $\theta = \frac{T-T_{main}}{T_{cool}-T_{main}}$ is the non-dimensional temperature, where T_{main} is the main flow inlet temperature and T_{cool} is the coolant temperature. The turbulent diffusivity α_t is usually calculated through the Reynolds analogy with a fixed turbulent Prandtl number as $\alpha_t = \nu_t / Pr_t$, where ν_t is the eddy viscosity.

GDH relies on several assumptions. As Corrsin [1] noted, GDH is only applicable in regions where the local scalar gradient is representative of the average gradient over the turbulent length scale. Therefore, in regions where the curvature

of the temperature distribution changes significantly over the turbulent length scale, gradient transport is not an appropriate model.

Furthermore, using a fixed Pr_t to calculate the turbulent diffusivity from the eddy viscosity depends on the validity of the Reynolds analogy between turbulent momentum and scalar transport. Typically, a default value of $Pr_t = 0.85$ is prescribed based on the value for a flat plate boundary layer. However, studies by Ling et al. [2] in a slot film cooling configuration and by He et al. [3] for discrete hole film cooling showed that the adiabatic effectiveness results were sensitive to the value of Pr_t used, and that more accurate results were provided by significantly lower values (0.2-0.45) of Pr_t.

Other studies have suggested that allowing spatial variation in Pr_t may enable improved predictive accuracy. Kohli and Bogard [4] performed experiments that showed that Pr_t varied significantly (by a factor of 4) spatially in their film cooling configuration. Lakehal [5] analyzed Direct Numerical Simulation (DNS) results for channel flow and flat plate boundary layer flow and showed that Pr_t changed significantly in the viscous sublayer, and proposed a model for film cooling flows that accounted for this spatial variation in Pr_t. Liu et al. [6, 7] investigated the effect of the prescribed Pr_t on the film cooling effectiveness and proposed a model which incorporated spanwise variation in Pr_t. They reported improved thermal predictions with this laterally varying Pr_t model.

Another key simplification of GDH is that it assumes that the turbulent diffusivity is isotropic. Kaszeta and Simon [8] measured the Reynolds stresses in a configuration with a row of film cooling holes and reported significant anisotropy in the eddy viscosity. This result suggests that it may be appropriate to use anisotropic models for the turbulent scalar fluxes in film cooling flows. Several such models have been proposed. Bergeles et al. [9] proposed a simple correction that includes anisotropy in the near wall region for film cooling flows. Lakehal [5] and Liu et al. [6] implemented this correction and reported improved adiabatic effectiveness predictions in their film cooling flows.

The Generalized Gradient Diffusion Hypothesis (GGDH) of Daly and Harlow [10], shown in Eqn. 2, incorporates anisotropy by including dependence on the individual Reynolds stress components. In this equation, C_{GGDH} is a model parameter that replaces the turbulent Prandtl number and τ is the turbulent time scale, commonly taken to be k/ε.

$$\overline{u_i'\theta'}_{GGDH} = -C_{GGDH}\tau\,\overline{u_i'u_j'}\frac{d\bar{\theta}}{dx_j} \tag{2}$$

Abe and Suga's [11] Higher Order Generalized Gradient Diffusion Hypothesis (HOGGDH) was developed to more accurately predict the streamwise component of the scalar fluxes by using quadratic products of the Reynolds stresses, as shown in Eqn. 3.

$$\overline{u_i'\theta'}_{HOGGDH} = -C_{HOGGDH}\frac{\tau}{k}\overline{u_i'u_k'}\;\overline{u_k'u_j'}\frac{d\bar{\theta}}{dx_j} \tag{3}$$

These higher order algebraic closures have the potential to be more accurate than GDH, since they incorporate anisotropy

into their predictions, but the accuracy of the anisotropy predictions is dependent on the accuracy of the Reynolds stress predictions. These models must either be paired with an algebraic stress model or a Reynolds Stress Transport Model (RSTM) for the flow. Such models often result in poor convergence, more stringent grid quality requirements, and increased computational cost. It is therefore only worth using GGDH or HOGGDH if they give significantly improved predictions.

Gorle et al. [12, 13] investigated a flow with scalar injection by a jet in supersonic crossflow and compared RANS results using GDH, GGDH, and HOGGDH to LES results. In this flow, none of the RANS models accurately predicted the scalar concentration distribution. However, it was not clear if this deficiency was due to the insufficiency of the scalar flux models, or to inaccuracies in the predicted Reynolds stresses, which were calculated through the k-ω SST model. Since this model does not predict anisotropy in the Reynolds stresses, it may have been ill-suited to evaluate the benefits of using an anisotropic turbulent scalar flux model.

Xueying et al. [14] implemented an anisotropic algebraic eddy viscosity model paired with a scalar flux model based on HOGGDH. They reported improved predictions for the adiabatic effectiveness in a discrete hole film cooling configuration. Rajabi-Zargarabadi and Bazdidi-Tehrani [15] ran a RSTM with both GDH and GGDH and showed that GGDH gave improved predictions in comparison to GDH. Azzi et al. [16] tested an anisotropic model based on GGDH for a film cooling flow and showed improved lateral spreading predictions in comparison to isotropic models. These studies agree that anisotropic algebraic closures for the scalar fluxes can give significantly improved film cooling effectiveness predictions. However, in all these studies, analysis of the turbulent scalar flux predictions was clouded by errors in the predicted Reynolds stresses. While RSTMs can often predict more accurate Reynolds stress fields than simple two-equation models, they still have uncertainty in these predictions, which would propagate through to the scalar flux predictions. It would therefore be useful to analyze the turbulent scalar fluxes and temperature distribution predicted by various models when the correct Reynolds stresses and mean velocity field are known.

In this paper, results from a high-fidelity LES of a discrete hole film cooling flow performed by Bodart et al. [17] are used to evaluate GDH, GGDH, and HOGGDH without the compounding effects of errors in the Reynolds stresses and velocity field. These LES results have been validated extensively [17] against the experimental results of Coletti et al. [18, 19] and have been shown to be in excellent agreement with the experimental data. The simulations provide all three components of the turbulent scalar fluxes and all six of the Reynolds stresses throughout the 3-dimensional computational domain. Such extensive results would have been impossible to obtain experimentally. Furthermore, the subgrid turbulent diffusivity and viscosity were an order of magnitude less than the molecular diffusivity and viscosity throughout the jet region [17], indicating that the LES subgrid model had only a negligible impact on the simulation results. Therefore, this paper will treat these LES results as data against which to compare the algebraic scalar flux model predictions. The objective of this paper is to use the LES results to isolate the effects of the turbulent scalar flux models in order to determine in which regions of the flow various RANS modeling assumptions are invalid and what effect those assumptions have on the predicted temperature distribution.

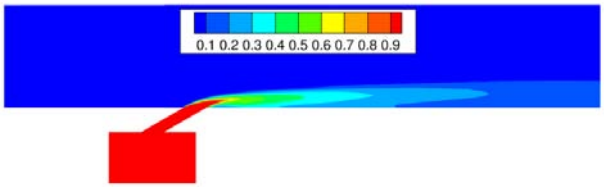

(a) FLOW CONFIGURATION WITH CONTOURS OF $\overline{\theta}$. COOLANT PLENUM AND INJECTION HOLE SHOWN.

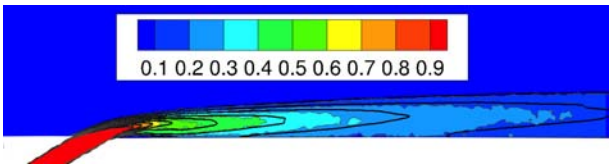

(b) COMPARISON OF LES AND EXPERIMENTAL RESULTS IN NEAR-INJECTION REGION. COLOR CONTOURS OF θ SHOWN ON THE CHANNEL CENTER-PLANE, AS MEASURED BY COLETTI ET AL. [18, 19]. CORRESPONDING ISOCONTOUR LINES FROM LES SHOWN IN BLACK.

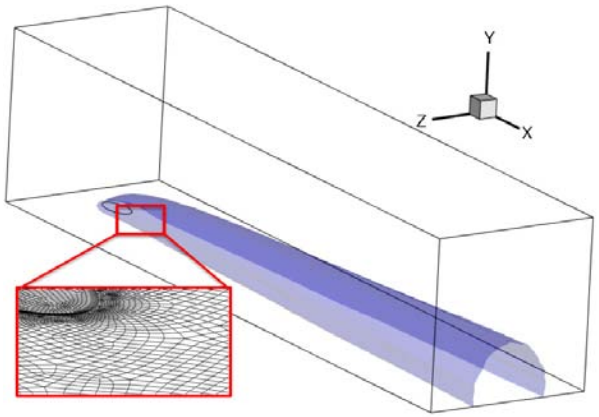

(c) RANS DOMAIN. ZOOMED-IN SECTION OF MESH SHOWN IN REGION NEAR HOLE EXIT. ISOSURFACE OF $\overline{\theta} = 0.01$ ALSO SHOWN FOR REFERENCE

Fig. 1. SCHEMATIC OF FLOW CONFIGURATION

1 Flow Configuration

The flow configuration is shown schematically in Fig. 1(a). It consists of a square test channel 8.62 D across, where D is the injection hole diameter. There is a single film cooling hole, angled 30° from horizontal, fed from a rectangular plenum underneath the channel.

The Reynolds number based on the hole diameter and bulk-averaged main flow velocity was 3,000. The flow was in the incompressible regime and the density ratio was 1.0, such that the fluid temperature could be treated as a passive scalar. Therefore, θ can also be thought of as the coolant concentration. The velocity ratio between the coolant flow and main flow was 1.0.

A detailed explanation of the computational set-up for the LES can be found in Ref. [17]. The LES was performed using CharLESx , a nominally second order, unstructured, finite-volume solver of the compressible Navier Stokes equations, developed at the Center for Turbulence Research at Stanford University. The Vreman subgrid scale model was used in

conjunction with a fixed subgrid turbulent Schmidt number of 0.9. The computational domain was highly resolved, consisting of 52 million hexahedral cells. *A posteriori* analysis showed that the subgrid turbulent viscosity and turbulent diffusivity were an order of magnitude lower than the molecular viscosity and diffusivity throughout most of the domain. This analysis demonstrated that the LES resolved most of the energy containing scales.

Bodart et al. [17] validated the LES results against experimental results collected by Coletti et al. [18, 19]. In order to parameterize and validate the synthetic turbulence injected at the inflow of the LES, Coletti et al. measured the Reynolds stresses and mean velocity using Particle Image Velocimetry (PIV) in three streamwise planes upstream of injection. Excellent agreement between these experimental results and the LES results at the same planes validated the turbulent inflow conditions used in the LES. Furthermore, Coletti et al. measured the full 3D mean coolant concentration distribution and the full 3D 3-component mean velocity field using Magnetic Resonance Imaging (MRI) techniques. Bodart et al. [17] performed detailed comparisons of the LES results and the experimental data for the mean scalar distribution and the mean velocity field, both in the hole and in the test channel. Figure 1(b) shows contours of θ on the channel center-plane as measured experimentally by Coletti et al. [18, 19], overlaid with isocontour lines from the LES results. This comparison demonstrates the close agreement between the LES and experimental results. These LES results are therefore considered well-validated and will be used as a reference against which to compare the various RANS scalar flux models throughout the rest of this paper.

2 RANS Computational Methods

The RANS domain is shown in Figure 1(c). It comprises the full channel cross section from $x = -3D$ to $x = +34D$, where the streamwise coordinate x is measured from the hole center. The RANS domain did not include the film cooling plenum or the angled hole since the coolant concentration in those regions was 100%. Figure 1(c) also includes a 1% isosurface of $\overline{\theta}$ showing that the domain boundaries are well beyond the region of interest.

The RANS solver was only used to solve the Reynolds averaged advection diffusion equation for the fluid temperature distribution, not the RANS equations themselves. The LES results for the mean velocity field and the Reynolds stresses were interpolated onto the RANS mesh.

A boundary condition of $\theta = 1.0$ was imposed at the hole exit. This boundary condition is consistent with the LES and experimental results, which showed no main flow ingestion into the hole. While the LES domain included the hole and plenum in order to calculate the velocity field, these regions could be excluded from the RANS calculations of the temperature distribution, since $\theta = 1.0$ everywhere in the hole and plenum. The main flow inlet was set 3 D upstream of the hole center, where a boundary condition of $\theta = 0.0$ was prescribed, since no coolant is expected to flow upstream. On the side, top, and bottom walls, an adiabatic condition was prescribed. A Neumann condition of zero streamwise gradient was specified at the outlet, 34 D downstream of the hole center.

The mesh consisted of 4.7 million hexahedral cells. A boundary layer mesh was used on the bottom wall with the first cell located at $y^+ \approx 2$. A section of this mesh is shown in Fig. 1(c). Second order upwind discretization was used in the thermal transport equation. At convergence, the residuals were less than 10^{-7}.

Three different algebraic closures for the turbulent scalar fluxes were applied: GDH, GGDH, and HOGGDH. The calculations with GGDH diverged, so the predicted temperature distribution is only available using GDH and HOGGDH. Direct assessment of the GGDH predictions for the turbulent scalar fluxes was still possible.

3 Results

3.1 Extracting α_t, ν_t and Pr_t from LES results

In LES, the large scale turbulence structures are time-resolved and the associated turbulent scalar fluxes do not require a closure. Therefore, α_t and ν_t are not calculated directly in LES. However, it is possible to extract isotropic values of the turbulent diffusivity and turbulent viscosity from the LES results, and use those to calculate a spatially-varying turbulent Prandtl number [20], as shown in Eqns. 4-6. In Eqn. 4, S_{ij} is the mean strain rate tensor.

$$\nu_{t,LES} = \frac{-\overline{u_i' u_j'} S_{ij} + \frac{2}{3} k \delta_{ij} S_{ij}}{2 S_{kl} S_{kl}} \tag{4}$$

$$\alpha_{t,LES} = \frac{-\overline{u_i' \theta'} \frac{d\bar{\theta}}{dx_i}}{\frac{d\bar{\theta}}{dx_j} \frac{d\bar{\theta}}{dx_j}} \tag{5}$$

$$Pr_{t,LES} = \frac{\nu_{t,LES}}{\alpha_{t,LES}} \tag{6}$$

As shown in Eqn. 4, the isotropic turbulent viscosity is calculated from the LES results by performing a weighted average of the turbulent viscosity that would yield each component of the LES Reynolds stresses, given the known mean strain rate tensor. The weighting is based on the strain rate tensor components. Similarly, in Eqn. 5, the isotropic turbulent diffusivity is given by the weighted average of the diffusivity in each direction, where the weights are the thermal gradients. This weighting makes sense because according to GDH, the effect of the turbulence on the scalar mixing in a given direction is directly proportional to the scalar gradient in that direction.

Figure 2 shows contours of $\nu_{t,LES}$, $\alpha_{t,LES}$ and $Pr_{t,LES}$ in streamwise slices spaced $4D$ apart. In these plots, $\alpha_{t,LES}$ and $\nu_{t,LES}$ are normalized by the bulk-averaged main flow velocity U_b and the hole diameter D. The contours are cut off for $\bar{\theta} < 0.01$. Furthermore, the contours of $\alpha_{t,LES}$ and $Pr_{t,LES}$ are blanked in regions where $D|\nabla\bar{\theta}| < 0.1$, since $\alpha_{t,LES}$ and $Pr_{t,LES}$ are not well-defined in regions where the thermal gradient goes to zero.

If the Reynolds analogy were true, the contours of $\alpha_{t,LES}$ would match those of $\nu_{t,LES}$, such that $Pr_{t,LES}$ would be constant in space. As Fig. 2 reveals, the Reynolds analogy breaks down in many regions of the flow, particularly near injection, where $Pr_{t,LES}$ decreases to values near 0.2. This breakdown in the Reynolds analogy could be due to the strongly localized change in fluid temperature near injection. In this region, Corrsin's [1] condition for the gradient transport being applicable could be violated, since the turbulent length scale could be of the same order as the distance over which the curvature of the temperature distribution changes. Based on this analysis, it seems likely that GDH with a fixed Pr_t will not be able to correctly predict the turbulent mixing in the near-injection region ($x/D < 4$).

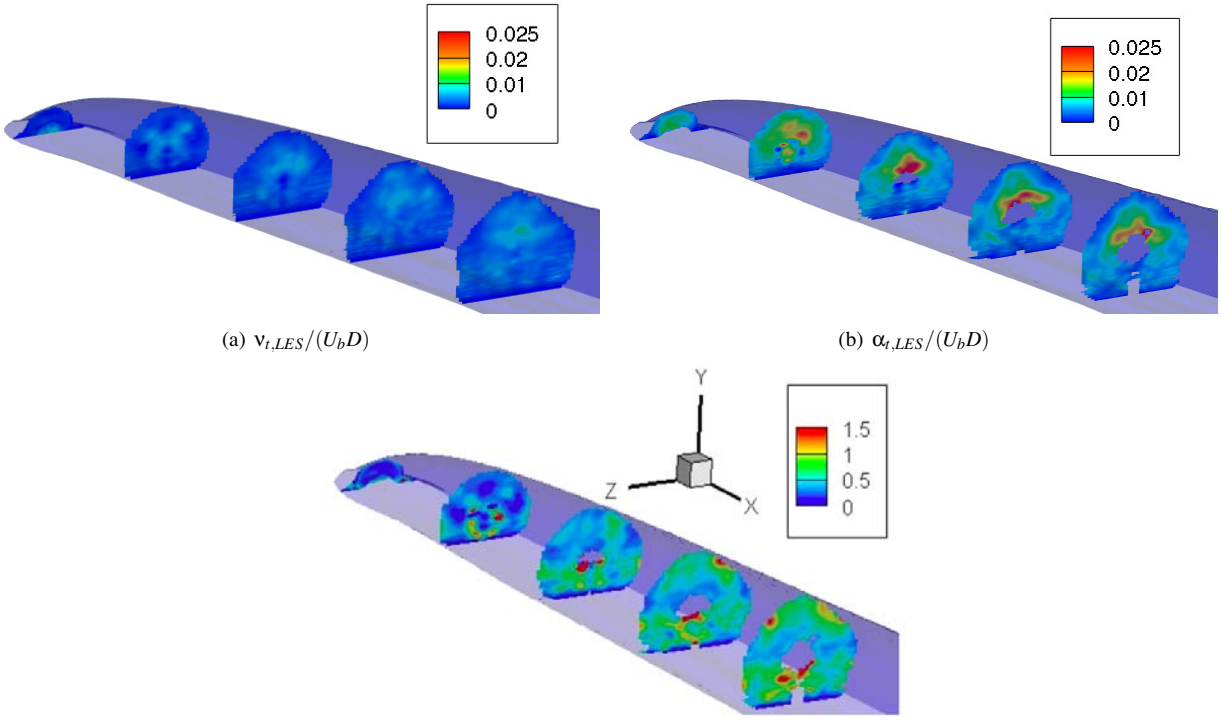

(a) $\nu_{t,LES}/(U_b D)$ (b) $\alpha_{t,LES}/(U_b D)$

(c) $Pr_{t,LES}$

Fig. 2. CONTOURS OF $\nu_{t,LES}/(U_b D)$, $\alpha_{t,LES}/(U_b D)$, AND $Pr_{t,LES}$ IN STREAMWISE SLICES SPACED $4D$ APART. THE CONTOURS OF $\alpha_{t,LES}/(U_b D)$ AND $Pr_{t,LES}$ ARE BLANKED IN REGIONS WHERE $D|\nabla\bar{\theta}| < 0.1$. ISOSURFACE OF $\bar{\theta} = 0.01$ SHOWN FOR REFERENCE IN BLUE.

The turbulent Prandtl number also decreases significantly in the near wall region, for $y^+ < 15$. This result is consistent with that of Lakehal [5], who reported a sharp drop in Pr_t in the viscous sublayer. Ling et al. [2, 20] also reported lower values of Pr_t in the near wall region of their slot film cooling configuration. While both the turbulent viscosity and turbulent diffusivity go to zero at the wall due to the no-slip and no-penetration boundary conditions, Ling et al. showed that the turbulent mixing in the near wall region can still play a key role in the film cooling performance.

3.2 Comparison of GDH, GGDH, and HOGGDH predictions of the turbulent scalar fluxes

It is possible to take the LES results for the velocity field, temperature distribution, and Reynolds stresses and plug these directly into the GDH, GGDH, and HOGGDH models, as shown in Eqns. 1- 3. The predicted turbulent scalar fluxes can then be compared to the LES results to determine how accurate the predictions from each model are.

One way to compare these three models is by analyzing the direction of the predicted turbulent scalar flux vector. This can be investigated by calculating the angle ϕ between the predicted turbulent scalar fluxes and the LES fluxes. A model that correctly predicts the scalar flux anisotropy would yield an angle $\phi = 0$, and a model that predicts scalar fluxes in the exact opposite direction would yield $\phi = \pi$. This analysis has the benefit of being independent of the time scale formulation for τ and the values of the model coefficients Pr_t, C_{GGDH}, and C_{HOGGDH}, since those act only as scale factors and will not affect ϕ.

Figure 3 shows contours of ϕ from GDH, GGDH, and HOGGDH. Once again, the contours have been cut off in regions

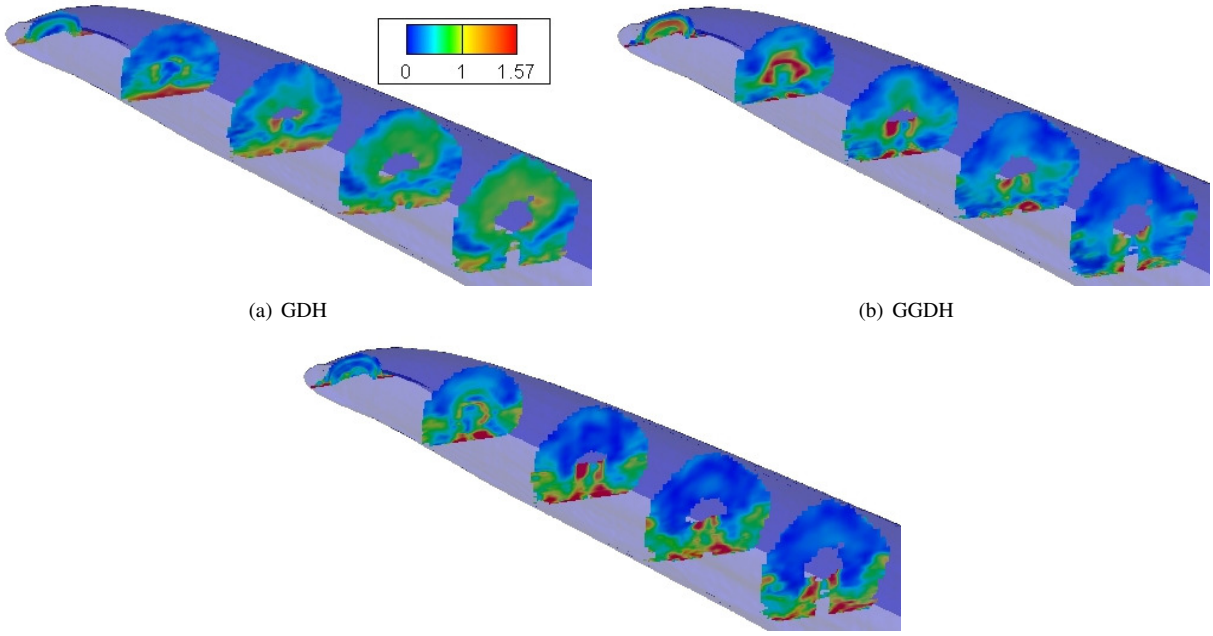

(a) GDH

(b) GGDH

(c) HOGGDH

Fig. 3. CONTOURS OF ϕ, THE ANGLE BETWEEN THE TURBULENT SCALAR FLUXES PREDICTED USING ALGEBRAIC CLOSURES AND THE LES TURBULENT SCALAR FLUXES. UNITS ARE IN RADIANS. THE SLICES ARE SPACED $4D$ APART, AND ARE BLANKED IN REGIONS WHERE $\overline{\theta} < 0.01$ OR $D|\nabla\overline{\theta}| < 0.1$. ISOSURFACE OF $\overline{\theta} = 0.01$ SHOWN FOR REFERENCE IN BLUE.

where $\theta < 0.01$ or $D|\nabla\overline{\theta}| < 0.1$. As can be seen in Fig. 3, none of the models correctly predict the scalar flux anisotropy everywhere in the flow. However, the GDH predictions show values of ϕ near $\pi/3$ ($60°$) for large regions of the flow near the top of the jet, particularly for $x/D > 8$. Incorrect modeling in this shear flow region could have a significant impact on how RANS predicts the mixing between the coolant flow and the main flow. Both GGDH and HOGGDH have improved predictions of the scalar flux anisotropy near the top of the jet. However, all three models struggle in the near wall region. This region of the flow is critical to correctly predicting the adiabatic film cooling effectiveness and heat transfer coefficient.

3.3 RANS predictions using the LES velocity field

RANS calculations were run using the LES velocity field and Reynolds stresses and implementing either GDH or HOGGDH as the closure for the turbulent scalar fluxes. For GDH, the turbulent diffusivity was prescribed in one of two ways: i) with α_t calculated using a fixed Pr_t and $\nu_{t,LES}$ or ii) using the $\alpha_{t,LES}$ extracted from the LES results. In the latter case, $\alpha_{t,LES}$ was constrained to be strictly positive to aid in convergence. This model will show the error incurred by restricting the turbulent diffusivity to be isotropic.

HOGGDH requires a turbulent time scale τ. Usually, $\tau = k/\varepsilon$ is used, but since LES does not provide the turbulent dissipation rate ε, a different time scale definition was required. For these calculations, τ was defined as: $\tau = \frac{1}{||S_{ij}||}$. Furthermore, values were needed for the model coefficient C_{HOGGDH}. In Abe and Suga's [11] channel flow calculation, they showed that $C_{HOGGDH} = 0.6$ was a reasonable value for this coefficient. From the LES results, a value for C_{HOGGDH} can also be extracted by calculating what value would give the correct magnitude for the turbulent scalar flux vector. This optimal value

was averaged over the entire 3-dimensional region for which $\theta > 0.01$, yielding a mean value of $C_{HOGGDH} = 1.5$. Since this value differed significantly from the value suggested in Abe and Suga, both values of the coefficient were tested. The difference between these values for C_{HOGGDH} could be due to the different time scale formulation used in this study.

Similarly, an optimal value of Pr_t could be extracted from the LES data by averaging $Pr_{t,LES}$ over the region with $\theta > 0.01$. This process yielded $Pr_t = 0.6$. Therefore, GDH was run with both $Pr_t = 0.6$ and $Pr_t = 0.85$, the latter being the default value for Pr_t. In all, five RANS cases were run. These cases are summarized in Table 1.

Figure 4 shows contours of $\overline{\theta}$ as calculated using RANS and LES. None of the RANS cases exactly match the LES results, particularly in the near wall region, where all of the RANS results over-estimate $\overline{\theta}$ near the centerline. Case 1, which uses the distribution of $\alpha_{t,LES}$ extracted from the LES results, has overall the closest match to LES. This similarity makes sense, since this model has the most information from LES–its only assumption is that the turbulent diffusivity is isotropic and positive. It does not represent a practical model that could be used in a general RANS case for which LES results are not available–it serves only to demonstrate how good GDH could be if it had all the right information. Even in this case, the RANS results are not perfect. The peak value of $\overline{\theta}$ in the jet core is over-predicted in the farther downstream region ($x/D > 12$). This over-prediction could be due to the fact that the turbulent diffusivity is not isotropic in that region. An examination of ϕ in Fig. 3(a) shows that the isotropic assumption is not accurate for large portions of the jet in the far downstream region.

In Cases 2 and 3, which rely on a fixed Pr_t, $\overline{\theta}$ is over-predicted in the near-injection region. This inaccuracy makes sense since it was previously shown, in Figure 2(c), that Pr_t should decrease significantly in this region.

In Case 4, HOGGDH with $C_{HOGGDH} = 0.6$ under-estimated the turbulent mixing. Using $C_{HOGGDH} = 1.5$, in Case 5, gave more accurate predictions, but the shape of the $\overline{\theta}$ distribution still differed from the LES results. This model gave the most accurate predictions for $\overline{\theta}$ in the jet core in the far downstream region.

A key quantity for film cooling applications is the adiabatic effectiveness, defined as $\eta = \frac{T_{aw}-T_{main}}{T_{cool}-T_{main}}$, where T_{aw} is the adiabatic wall temperature. η is given by the value of $\overline{\theta}$ at the wall. Contours of η are shown in Figure 5 for the LES and RANS results.

As Figure 5 demonstrates, all of the RANS models over-estimate the adiabatic effectiveness on the centerline. Even in Case 1, using the LES $\alpha_{t,LES}$, the adiabatic effectiveness is over-predicted. This result suggests that gradient transport is not an accurate model for this flow. Bodart et al. [17] reported counter-gradient diffusion in the region immediately downstream

Table 1. Turbulent Scalar Flux Models for RANS

Case #	Model	Parameter Value
1	GDH	$\alpha_t = \alpha_{t,LES}$
2	GDH	$Pr_t = 0.85$
3	GDH	$Pr_t = 0.6$
4	HOGGDH	$C_{HOGGDH} = 0.6$
5	HOGGDH	$C_{HOGGDH} = 1.5$

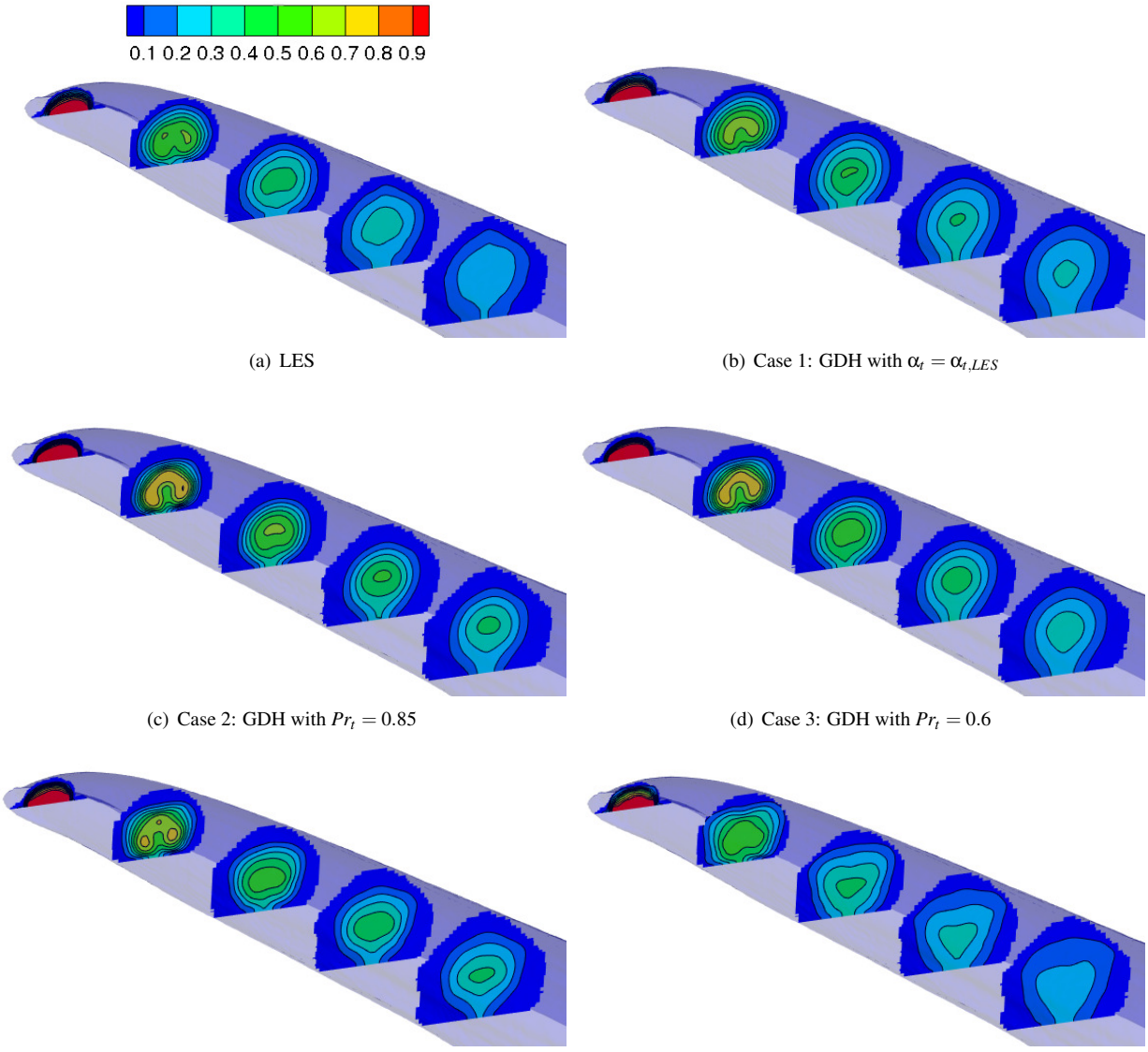

(a) LES

(b) Case 1: GDH with $\alpha_t = \alpha_{t,LES}$

(c) Case 2: GDH with $Pr_t = 0.85$

(d) Case 3: GDH with $Pr_t = 0.6$

(e) Case 4: HOGGDH with $C_{HOGGDH} = 0.6$

(f) Case 5: HOGGDH with $C_{HOGGDH} = 1.5$

Fig. 4. CONTOURS OF $\overline{\theta}$ IN STREAMWISE SLICES SPACED $4D$ APART FROM LES AND RANS. ISOSURFACE OF $\overline{\theta} = 0.01$ SHOWN FOR REFERENCE IN BLUE.

of injection. Since Case 1 restricted α_t to be positive in order to promote convergence, counter-gradient diffusion could be responsible for the difference between the RANS and LES results.

Figure 5 also shows that the GDH with a fixed Pr_t (Cases 2 and 3) tends to under-estimate the spanwise spread of the coolant along the bottom wall. HOGGDH with $C_{HOGGDH} = 1.5$ (Case 5) gives improved predictions of the spanwise variation in η. This result is consistent with those of Lakehal [5], Azzi et al. [16], and Xueying et al. [14]. In all three cases, increases in the predicted lateral spreading and improved accuracy were reported when anisotropic models were implemented for the turbulent scalar fluxes.

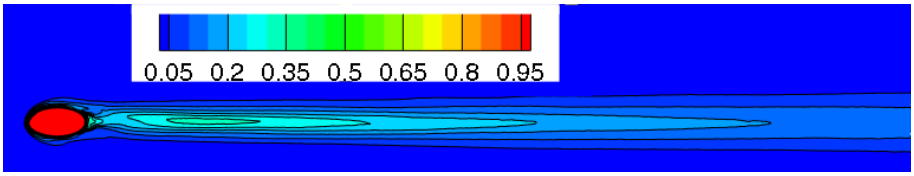

(a) LES

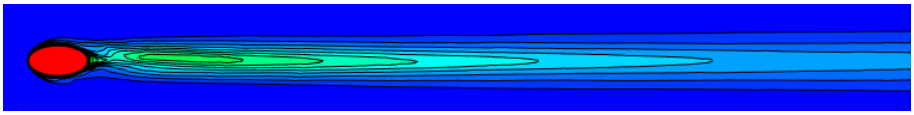

(b) Case 1: GDH with $\alpha_t = \alpha_{t,LES}$

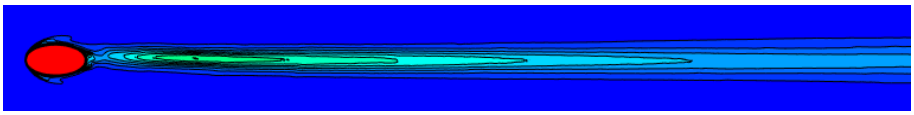

(c) Case 2: GDH with $Pr_t = 0.85$

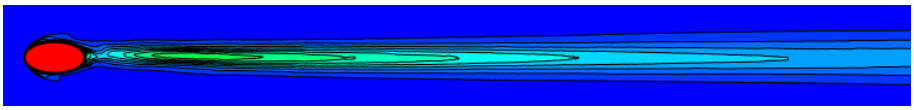

(d) Case 3: GDH with $Pr_t = 0.6$

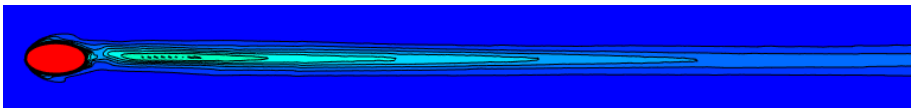

(e) Case 4: HOGGDH with $C_{HOGGDH} = 0.6$

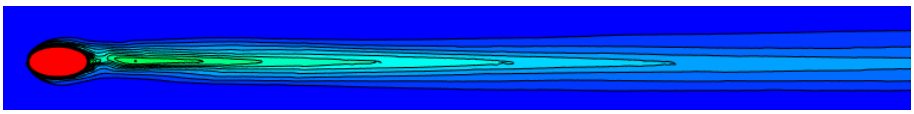

(f) Case 5: HOGGDH with $C_{HOGGDH} = 1.5$

Fig. 5. CONTOURS OF η ON THE BOTTOM WALL. THE REGION DEPICTED EXTENDS 30 D DOWNSTREAM OF INJECTION, AND $2D$ ON EITHER SIDE OF THE CENTERLINE.

3.4 Quantification of Model Error

In order to quantitatively compare the model predictions in these five cases, it is useful to employ a cost function, E. This cost function is defined as:

Table 2. Cost Function Evaluation for Different Turbulent Scalar Flux Models

Case #	E
1	0.013
2	0.034
3	0.023
4	0.031
5	0.020

$$E = \frac{1}{n}\sum_{i} |\overline{\theta_{RANS,i}} - \overline{\theta_{LES,i}}| \tag{7}$$

In Eqn. 7, the sum is over all the points for which $\overline{\theta_{LES}} > 0.01$, and n is the number of points within that region. E therefore represents the average error magnitude over the region where the coolant concentration is greater than 1%. This cost function is similar to that presented by Ling et al. [21]. It enables the quantitative comparison of three-dimensional distributions.

The cost function was calculated for all five RANS cases, and the results are shown in Table 2. The cost function evaluation shows that Case 1 has the closest match to the LES results. It also shows that the tuned HOGGDH (Case 5) does better than the tuned GDH with a fixed Pr_t (Case 3). However, tuning the coefficients makes a much bigger difference than switching from GDH to HOGGDH, as can be seen by comparing Case 2 to Case 3, or Case 4 to Case 5. These results suggest that it is not worth switching to HOGGDH unless it is possible to tune the model coefficient C_{HOGGDH}. While HOGGDH may give a better prediction of the scalar flux anisotropy, the magnitude may be far from correct without tuning C_{HOGGDH}.

4 Conclusions

Three algebraic closures for the turbulent scalar fluxes were evaluated for a film cooling configuration using high fidelity LES results. Distributions of the turbulent diffusivity, turbulent viscosity, and turbulent Prandtl number were extracted from the LES and analyzed. These results showed that the Reynolds analogy breaks down and that significantly lower values of the turbulent Prandtl number are required near injection and near the bottom wall.

The GDH, GGDH, and HOGGDH predictions of the scalar flux anisotropy were then investigated by calculating the angle between the modeled scalar fluxes and the LES scalar fluxes. GGDH and HOGGDH had more accurate predictions of the scalar flux anisotropy near the top of the jet, but all three models had high error in the near wall region at the bottom of the jet.

The LES velocity field and Reynolds stresses were fed into a RANS solver for the temperature distribution, using GDH and HOGGDH as scalar flux closures. Tuned model coefficients were extracted from the LES and the model performance was compared both with the default values of the coefficients as well as with the tuned values. It was shown that all models over-predicted the centerline adiabatic effectiveness downstream of injection. HOGGDH with a tuned model coefficient provided the best predictions of the lateral spread of the coolant jet.

By evaluating a quantitative cost function, it was possible to compare the three-dimensional temperature distributions predicted by the various RANS turbulent scalar flux models. This comparison revealed that tuning the model coefficients had a more significant impact on the temperature distribution predictions than changing from GDH to HOGGDH.

Based on these results, it is recommended that, whenever possible, model coefficients should be tuned using an LES, DNS, or experiment from a similar flow. In the case that it is not possible to tune the model coefficients, it seems as if

upgrading to HOGGDH from GDH may not be worth the extra challenge in implementing a RSTM and gaining convergence.

Acknowledgements

J. Ling was funded through an NSF graduate research fellowship at the time that this work was undertaken. K.J. Ryan and the LES work of J. Bodart are funded by Honeywell Corporation.

References

[1] Corrsin, S., 1974. "Limitations of gradient transport models in random walks and in turbulence". *Advances in Geophysics,* **18**, pp. 25–60.

[2] Ling, J., Elkins, C., and Eaton, J., 2014. "Optimal turbulent Schmidt number for RANS modeling of trailing edge slot film cooling". *J. Eng. Gas Turbines Power,* **doi: 10.1115/1.4029206**.

[3] He, G., Guo, Y., and Hsu, A., 1999. "The effect of Schmidt number of turbulent scalar mixing in a jet-in-crossflow". *International Journal of Heat and Mass Transfer,* **42**, pp. 3727–3738.

[4] Kohli, A., and Bogard, D., 2005. "Turbulent transport in film cooling flows". *Journal of Heat Transfer,* **127**, May, pp. 513–520.

[5] Lakehal, D., 2002. "Near-wall modeling of turbulent convective heat transport in film cooling of turbine blades with the aid of direct numerical simulation data". *Journal of Turbomachinery,* **124**, pp. 485–498.

[6] Liu, C., Zhu, H., and Bai, J., 2008. "Effect of turbulent Prandtl number on the computation of film cooling effectiveness". *International Journal of Heat and Mass Transfer,* **51**, pp. 6208–6218.

[7] Liu, C., Zhu, H., and Bai, J., 2011. "New development of the turbulent Prandtl number models for the computation of film cooling effectiveness". *International Journal of Heat and Mass Transfer,* **54**, pp. 874–886.

[8] Kaszeta, R., and Simon, T., 2000. "Measurement of eddy diffusivity of momentum in film cooling flows with streamwise injection". *J Turbomach,* **122**, January, pp. 178–183.

[9] Bergeles, G., Gosman, A., and Launder, B., 1978. "The turbulent jet in a cross stream at low injection rates: A three-dimensional numerical treatment". *Numerical Heat Transfer,* **1**, pp. 217–242.

[10] Daly, B., and Harlow, F., 1970. "Transport equations in turbulence". *Physics of Fluids,* **13**, pp. 2634–2649.

[11] Abe, K., and Suga, K., 2001. "Towards the development of a Reynolds-averaged algebraic turbulent scalar-flux model". *Journal of Heat and Fluid Flow,* **22**, February, pp. 19–29.

[12] Gorle, C., Emory, M., and Iaccarino, G., 2011. "Epistemic uncertainty quantification of RANS modeling for an underexpanded jet in a supersonic crossflow". *Center for Turbulence Research Annual Research Briefs*.

[13] Gorle, C., Emory, M., and Iaccarino, G., 2012. "RANS modeling of turbulent mixing for a jet in supersonic crossflow: model evaluation and uncertainty quantification". *Turbulence, Heat and Mass Transfer*.

[14] Xueying, L., Yanmin, Q., Jing, R., and Hongde, J., 2013. "Algebraic anisotropic turbulence modeling of compound angled film cooling validated by PIV and PSP measurements". *ASME Turbo Expo 2013*.

[15] Rajabi-Zargarabadi, M., and Bazdidi-Tehrani, F., 2010. "Implicit algebraic model for predicting turbulent heat flux". *International Journal for Numerical Methods in Fluids,* **64**, pp. 517–531.

[16] Azzi, A., and Lakehal, D., 2002. "Perspectives in modeling film cooling of turbine blades by transcending conventional two-equation turbulence models". *J. Turbomach,* **124**, pp. 472–484.

[17] Bodart, J., Coletti, F., Moreno, I. B., and Eaton, J., 2013. "High-fidelity simulation of a turbulent inclined jet in a crossflow". *CTR Annual Research Briefs 2013*.

[18] Coletti, F., Elkins, C., and Eaton, J., 2012. "Experimental investigation of turbulent flow and scalar transport in a inclined jet in crossflow". *7th International Symposium on Turbulence, Heat and Mass Transfer*, September.

[19] Coletti, F., Benson, M., Ling, J., Elkins, C., and Eaton, J., 2013. "Turbulent transport in an inclined jet in crossflow". *International Jounal of Heat and Fluid Flow,* **43**, pp. 149–160.

[20] Ling, J., Rossi, R., and Eaton, J., 2015. "Near wall modeling for trailing edge slot film cooling". *Journal of Fluids Engineering,* **137**.

[21] Ling, J., Coletti, F., Yapa, S., and Eaton, J., 2013. "Experimentally informed optimization of turbulent diffusivity for a discrete hole film cooling geometry". *International Journal of Heat and Fluid Flow,* **44**, pp. 348–357.